

MODELING REGIONAL SEISMIC PHASES AND CODA FROM EARTHQUAKES AND EXPLOSIONS  
USING GENERALIZED FOURIER METHODS IN 2D/3D

Jessie L. Bonner<sup>1</sup>, David G. Harkrider<sup>1</sup>, James Britton<sup>1</sup>, and Jeffrey L. Orrey<sup>2</sup>

Weston Geophysical Corp.<sup>1</sup> and GeoVisual Technologies, Inc.<sup>2</sup>

Sponsored by the National Nuclear Security Administration

Contract No. DE-AC52-05NA26610

Proposal No. BAA05-59

**ABSTRACT**

We continue to develop a numerical code for modeling regional seismic phases from earthquakes and explosions in 2D/3D media using Generalized Fourier Methods (GFM). During the past year, we have modified the GFM code by implementing efficient and accurate  $Q$  parameterization and variable gridding in order to simulate topography. The objective of our current modeling is to better understand  $Lg$  and  $Lg$  coda propagation using synthetics generated with both earthquake and explosion source models.

We have studied five velocity models as described in Yang (2002), including two Tibet models, a Chinese model, and a Tarim Basin model. We parameterized the models for 2D GFM with a grid spacing of 0.25 km, horizontal dimension of 962 km, and depth dimension of 110 km. We used a double couple source with and without attenuation to generate the synthetics. We estimated the geometrical spreading for  $Lg$  using the GFM synthetics without attenuation. We determined that  $Lg$  decays at a rate of  $\Delta^{-0.52}$  and  $\Delta^{-1.01}$  for spectral versus time domain measurements, which are similar to Yang's (2002) results for wavenumber-integration synthetics. We are currently examining the 3D effects on geometric spreading.

Next, we applied a  $Q_\beta=200$  and  $Q_\alpha=2.25*Q_\beta$  throughout the entire model and generated synthetics using the 2D GFM for source depths of 1, 5, 10, and 30 km. We then used the two-station technique (Xie et al., 2006) to estimate power-law  $Q_0$  and  $\eta$  from the synthetics. For all models and depths, the  $Q_0$ s estimated from the synthetics were within 5% of the input  $Q_\beta$ . With the exception of the two Tibetan models at a source depth of 1 km ( $\eta>0.4$ ), all frequency-dependence  $\eta$  results were  $\sim 0$ . The estimated  $Q_0$ s are all reduced when stochastic variations are added to the model. For example, when we add perturbations with von Karman distributions, 10% amplitudes, and 1 km correlation lengths, the  $Q_0$  is decreased from the input  $Q$  by 6-25%. The amount of reduction caused by the heterogeneities is both model and depth dependent.

In the process of porting source-time functions with our synthetics, we reviewed the available explosion source theories. We have included the Haskell (1961) source theory. Haskell suggested that simple analytical functions could fit the calculated reduced displacement potentials from near-source measurements of nuclear tests detonated in different lithologies. He showed that displacement scaling is inversely proportional to the cube root of yield at high frequencies and proportional to yield at low frequencies. The theory is based on continuum mechanics, which allows for either realistic plastic or fractured emplacement media. Additionally, it allows for different pressure and gas porosity considerations both above and below the water table. The theory also allows for different cavity and vapor radii, which could be used to model decoupled explosions. These and additional features of the Haskell source theory result in accurate predictions of the observed characteristics (e.g., corner frequencies,  $\psi_{\infty}$ , etc) of Nevada Test Site (NTS) explosions such as Cowboy and Rainier.

We modeled small chemical explosions and found that the Haskell-predicted  $M_w$ s are typically within 7% of the observed estimates based on moment tensor inversions. Haskell's source performed better at estimating the moment magnitudes than Denny and Johnson (1991), which was based on NTS data. Our next step is to convolve the Haskell source with the GFM synthetics to examine source effects on regional phase partitioning from explosions.

### OBJECTIVES

We continue to develop a numerical code for modeling regional seismic phases from earthquakes and explosions in 2D/3D media using Generalized Fourier Methods (GFM). During the past year, we have modified the GFM code by implementing efficient and accurate  $Q$  parameterization and variable gridding in order to simulate topography. The objective of our current modeling is to better understand  $Lg$  and  $Lg$  coda propagation using synthetics generated with both earthquake and explosion source models.

### RESEARCH ACCOMPLISHED

#### **Code Improvements**

**Anelasticity.** We have successfully implemented anelastic attenuation ( $Q$ ) in the GFM with parallelization. The  $Q$  implementation makes use of a time-domain approximation of frequency-dependent attenuation through a superposition of relaxation mechanisms (Emmerich and Korn, 1987). In order to apply this technique in the parallel computation environment used with GFM, it was necessary to extend the Message Passing Interface (MPI) calls to the additional “memory variables” that make up the relaxation mechanism contributions to the stress tensor. Our  $Q$  implementation is completely general, in that it is possible to assign independent  $Q_p$  and  $Q_s$  values, for  $P$ -waves and  $S$ -waves, respectively, to each node in the 3D computational grid. This requires significant additional memory since the memory variables are stored for all nodes in 3D, but it affords the most detailed specification of  $Q$  models. In future efforts, we can consider reducing the number of independent  $Q$  values stored in the grid to less than the total number of computational nodes in the model, where a simplified  $Q$  structure will suffice and significant memory savings will allow us to run simulations to greater distances and/or to high frequencies.

There is some computational complexity added by the parallelization of the  $Q$  implementation, in that since each computational node has a (potentially) unique  $Q$  value and those values must be read into memory for each processor that is assigned the associated sub-region of the computational grid. We store the  $Q$  structure of the Earth model along with the other model parameters (i.e.,  $V_p$ ,  $V_s$  and density), and then we read all material values using the master processor, which in turn distributes the material values for each sub-region associated with each slave processor to begin time step iterations.

**Non-uniform Grid for Topography.** We have successfully implemented an irregularly-spaced grid into GFM in the vertical coordinate direction – a final step in demonstrating the generalized technique of applying a coordinate transformation to the computation grid to simulate non-regular physical spaces such as a topographic surface (Orrey, 1995). The practical application of an irregular vertical grid spacing is to improve the accuracy of the solutions for signals affected by the free surface (i.e., fundamental and higher mode surface waves –  $Rg$ ,  $Lg$ , etc.). The improvement is realized by reducing the computational node spacing near the free surface so that signals near the surface are spatially sampled with relatively more nodes. The denser grid spacing (in the vertical direction) better supports the curvature of the wavefront near the surface and the interaction of the wavefront with the boundary.

The other practical advantage of using a non-uniform grid in the vertical direction is to save grid points (and therefore, memory). For most Earth models of interest, the relatively lower velocity values near the surface require higher spatial sampling for a maximum solution frequency of interest due to the relatively higher wavelengths in the low velocity zone. Therefore, using a smaller grid spacing in the low velocity zone only, versus throughout the entire grid, is a more efficient implementation.

In our final task to implement surface topography, we will extend the non-uniform grid formulation to the case where the vertical grid point distribution is also a function of the horizontal coordinates. Then the grid can be “stretched” and “compressed” in the vertical direction as needed to match the topography of the region of interest.

### Examining the Effects of Crustal Heterogeneity on Regional Phases

In his paper examining the geometric spreading of  $Lg$ , Yang (2002) studied five velocity models, including a primary model (Levin et al., 1995), two Tibet models (Jih, 1998; Li and Mooney, 1998), a Chinese model (Jih, 1998), and a Tarim Basin model (Jih, 1998). The reader is referred to Yang's (2002) Figure 1 and Table 1 for the models. We parameterized the Yang (2002) models for the two-dimensional version of GFM (2D GFM) with a grid spacing of 0.25 km, horizontal dimension of 962 km, and depth dimension of 110 km. We used a double couple source with and without attenuation to generate the synthetics. For models with attenuation, we applied a  $Q_{\beta}=200$  and  $Q_{\alpha}=2.25*Q_{\beta}$  throughout the entire model and generated synthetics using 2D GFM for source depths of 1, 5, 10, and 30 km. We have also added stochastic variations to the media to examine the effects of crustal heterogeneity of regional phases. For this study, we added perturbations with von Karman distributions, 10% and 20% amplitudes, and 1 km horizontal and vertical correlation lengths.

Example of the synthetics from a 10 km deep double couple earthquake source propagated through homogenous and heterogeneous versions of the China model (Jih, 1998) at a distance of 500 km are shown in Figure 1. The phases are highlighted by group velocity windows, which for  $Lg$  (e.g., 3.72 and 3.12 km/sec) were taken from Yang (2002). Spectral ratios were formed between the homogenous model synthetic (top in Figure 1) in the numerator and the synthetics for the two heterogeneous models (Figure 2) in the denominator. The effect of the random perturbations is to decrease the amplitudes of the direct arrivals  $Pn$ ,  $Pg$ , and  $Lg$  at frequencies above 0.5 Hz. The energy from these direct phases is scattered into the  $P$  coda (Figure 2) and  $Lg$  coda (not shown on Figure 2 but obvious from Figure 1). While this is expected, we did not expect to see that the amplitudes for the short-period surface waves (e.g.,  $Rg$ ) are increased by a factor of 2-3x for the models with the stochastic variations between 0.5 and 1.5 Hz. It is generally thought that  $Rg$  would be highly scattered into  $S$ -waves or coda.

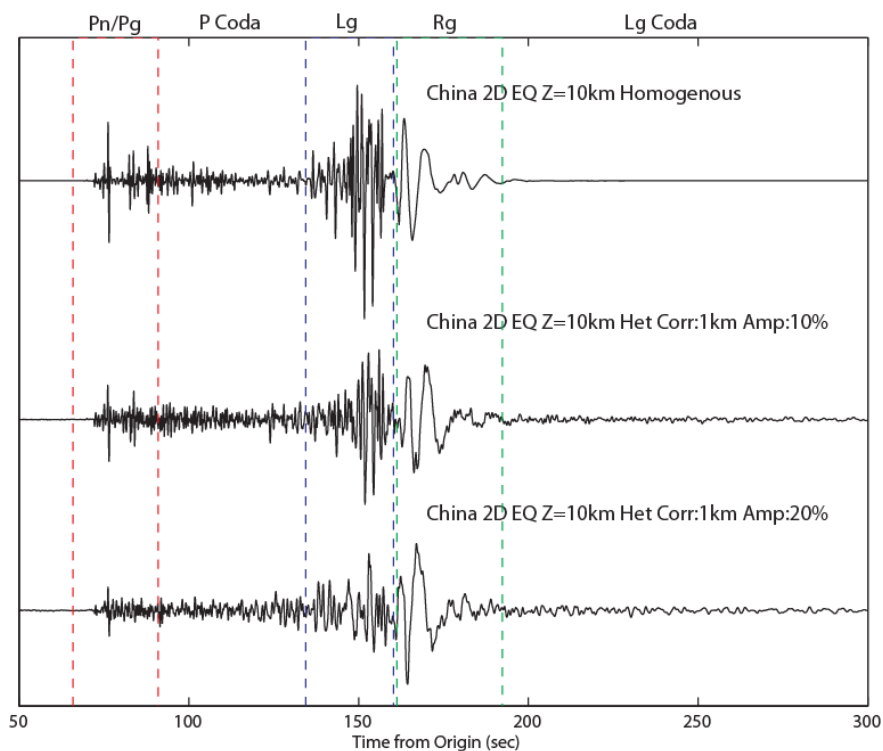


**Figure 1. 2D GFM synthetics for a China model (Jih, 1998) at a distance of 500 km. The model for the upper trace had no stochastic variations, while the lower two traces were propagated through a model with stochastic variations with amplitudes of 10% (middle) and 20% (bottom). The regional phases are highlighted by dashed lines.**

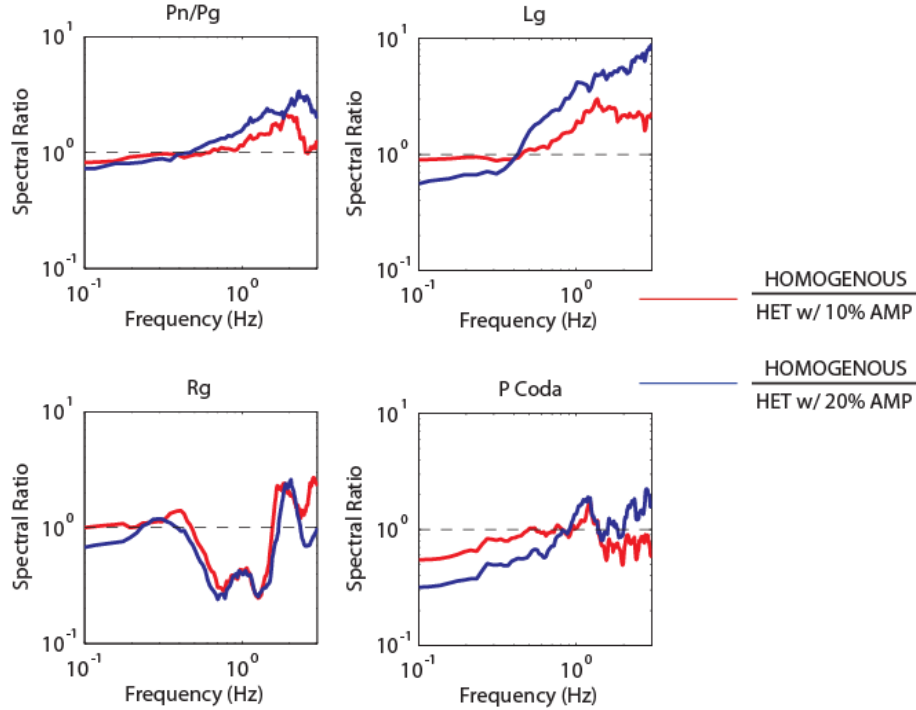


**Figure 2. Spectral ratios for the regional phases shown in Figure 1. In each case, the signal in the numerator is from synthetics propagated through a homogenous model while the signal in the denominator is from the heterogeneous model. The red and blue lines represent 10% and 20% stochastic perturbations, respectively.**

The next stage of modeling involved quantifying the effects of heterogeneity on  $Lg Q$ . The synthetic  $Lg$  were windowed using a group velocity window based on Yang (2002). Pre-event noise was similarly windowed, and Fourier spectra of synthetic noise and  $Lg$  were calculated. Assuming that  $Lg Q$  follow the power-law frequency dependence of  $Q = Q_0 f^\eta$  (where  $Q_0$  is the  $Lg Q$  at 1 Hz and  $\eta$  is the frequency dependence), the interstation  $Q$  can be estimated using Xie et al. (2004, 2006):

$$\ln \left\{ \frac{V_{Lg}}{\pi \Delta_{i,j}} \ln \left[ \frac{\Delta_i^{1/2}}{\Delta_j^{1/2}} \times \frac{A_i(f)}{A_j(f)} \right] \right\} = (1 - \eta) \ln f - \ln Q_0, \quad (1)$$

where  $V_{Lg}$  is the typical  $Lg$  group velocity of 3.5 km/sec,  $\Delta_i$  and  $\Delta_j$  are the epicentral distances to the two aligned stations where the  $Lg$  spectra  $A_i(f)$  and  $A_j(f)$  were observed, and  $\Delta_{i,j}$  is the interstation distance. In Equation 1, the left hand quantity is calculable from the observed spectral ratios and can be averaged over repeating two-station paths to provide stable estimates of  $Q_0$  and  $\eta$  by a linear regression.

We used Equation 1 to estimate  $Lg Q_0$  and  $\eta$  for all possible two-station combinations of the GFM synthetics with interstation separation greater than 200 km. We considered frequencies between 0.1 and 2 Hz due to the accuracy limitations of GFM and a 0.25 km grid spacing. Figure 3 shows the estimated  $Lg Q$  and  $\eta$  as a function of the interstation distance for the China model and a synthetic earthquake at 10 km depth. For this model, inclusion of the stochastic variations reduced the average estimated  $Q_0$  from 202 to 178 (10% perturbation of amplitudes) to 146 (20%). The error in the estimated values increases at shorter interstation distances, which was theorized in the Appendix of Xie et al. (2004). Also of interest is the change in the frequency dependence when increasing the amplitude of the stochastic variations. The mean  $\eta$  ranges from -0.1, which, when the error is considered could be assumed to be frequency independent, to 0.5 for the stochastic model with 20% amplitude perturbations. This later value is similar to what is often observed on real seismic data.

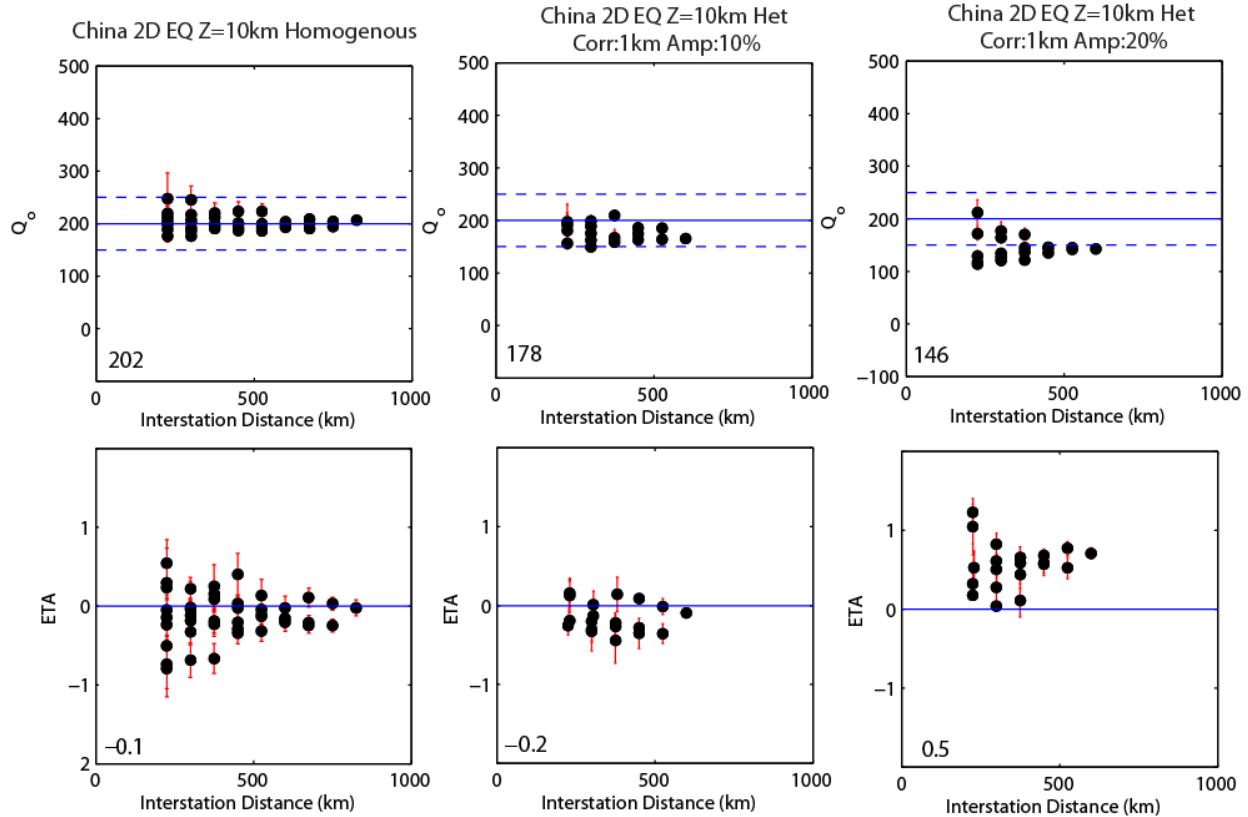


**Figure 3.** Two-station  $Lg Q_o$  and  $\eta$  (ETA) processing for a synthetic earthquake at 10 km depth and a China velocity model (Jih, 1998) without (left column) and with stochastic variations (middle and right columns). The initial shear-wave  $Q_\beta$  value of the crust was set to 200 (solid blue line in upper plots with  $\pm 20\%$  shown as dashed lines), and we expected no frequency dependence in the results (e.g.,  $ETA=0$ ; blue line in lower plots). Each  $Lg Q_o$  and ETA value shows the error as a vertical red line. Mean values are listed in the left corner of each plot.

Figure 4 shows the results for all models except the Tarim Basin model. The very low velocities coupled with the low  $Q_\beta$  in this model resulted in instabilities in GFM, which are currently being investigated. The problem is asymptotic drift of the synthetics at simulation times greater than 100 seconds. For all other homogenous models and depths, the  $Q_o$ s estimated from the synthetics were within 5% of the input  $Q_\beta$ . With the exception of the two Tibetan models at a source depth of 1 km ( $\eta > 0.4$ ), all frequency-dependence  $\eta$  results were  $\sim 0$ .

The estimated  $Q_o$ s are reduced when stochastic variations are added to the model. For example, when we add perturbations with von Karman distributions, 10% perturbation amplitudes, and 1 km correlation lengths, the  $Q_o$  is decreased from the input  $Q_\beta$  by 10–25%. The amount of reduction caused by the heterogeneities is both model and depth dependent. For example, the “primary” model shows the largest decrease in the  $Q_o$  estimates for synthetic earthquakes at 1, 5, and 10 km depths; however the estimate for the 30 km deep source is anomalously above the input  $Q_\beta$  value. There is currently no explanation for this observation, as it does not appear to be measurement error.

Adding the stochastic variations with 10% perturbation amplitudes to the velocity models has little effect on the frequency dependence of the synthetic  $Lg$ . However, increasing the perturbation amplitude to 20% increases the frequency dependence from  $\sim 0$  to positive values as large as 0.9 depending on source depth. The  $Q_o$  is decreased from the input  $Q_\beta$  by 10–40% for the models with the larger amplitude perturbations. These synthetic results have important implications as to how  $Lg Q_o$  and  $\eta$  estimates from observed seismic data should be interpreted.

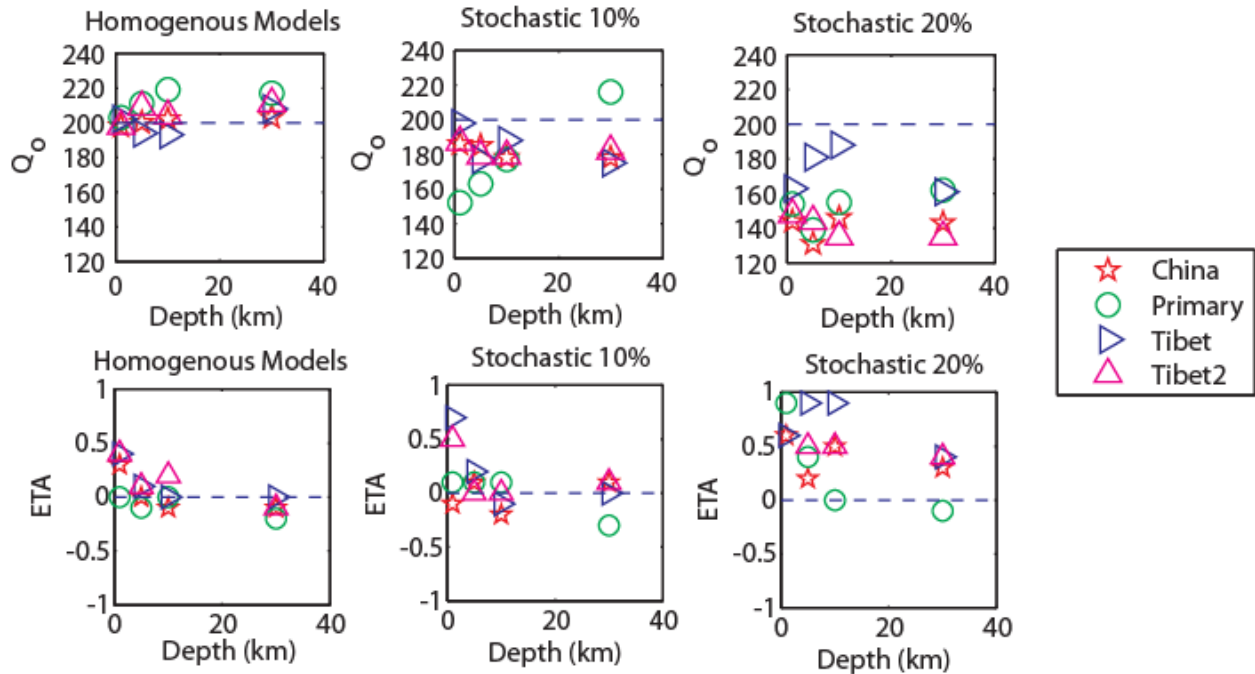


**Figure 4.** Two-station  $L_g Q_o$  and  $\eta$  (ETA) processing for a synthetic earthquakes at depths of 1, 5, 10, and 30 km for four different models without (left column) and with stochastic variations (middle and right columns). The initial shear-wave  $Q_\beta$  value of the crust was set to 200 (dashed blue line in upper plots). No frequency dependence (e.g.,  $ETA=0$ ) is shown as the dashed line in the lower subplots.

### 3D Simulations for the NTS

Bonner et al. (2008) examined earthquake and explosion synthetics for 2D GFM models for the NTS region. We are currently extending this modeling to 3D GFM. The background velocity structure for NTS is based on a regional model for the Basin and Range similar to the model developed by Benz et al. (1991). The velocities in the upper crust are based on borehole data, geologic and gravity data, refraction studies and seismic experiments. We have used various techniques to estimate stochastic parameters for the Basin and Range. This includes using previous well-located nuclear explosions to estimate correlation lengths for scattering of the  $L_g$  phase (Tibuleac et al., 2006). These results suggest that the horizontal correlation lengths for a von Karman stochastic model range between 0.5–2 km with smaller vertical correlation lengths. The Hurst numbers (H) are related to the fractal dimension of the medium and range between 0.3 and 0.6. Bonner et al. (2008) obtained their best 2D modeling results using the Patton and Taylor (1984) attenuation model, which is characterized by low  $Q_\beta$  (85–172) throughout the entire crust. We have used the Patton and Taylor (1984)  $Q$  model in the 3D synthetic runs.

Figures 5 and 6 present several different synthetic seismograms recorded at 200 km propagated through a 3D model with grid spacing of 0.5 km. For the stochastic model runs, we considered horizontal and vertical correlation lengths of 2 km, with smaller correlation length simulations planned. For reference, we plot wavenumber-integration synthetics (Herrmann, 2002) for 1D homogenous versions of the 3D model. Finally, we show an NTS explosion recorded at Mina, Nevada (MNV) at a distance of 201 km.

While we await the results for smaller correlation lengths, it is clear that adding stochastic variations to the NTS model provides a better match to the observed NTS data. The large amplitude explosion-generated  $R_g$  predicted by the wavenumber-integration synthetics in Figure 5 is not visible in the Mast waveform at MNV. The phase has also been scattered in the GFM synthetics with stochastic variations. The GFM synthetics also predict the larger amplitude phase—possibly higher mode surface waves—at MNV just after the  $L_g$  window, although the observed arrival appears to be lower frequency than the synthetics.

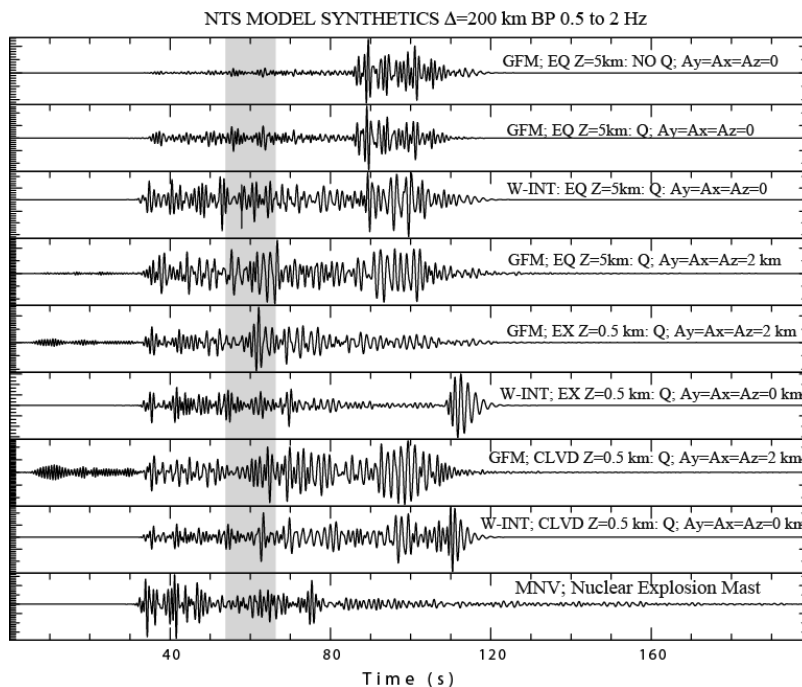


Figure 5. 3D GFM and 1D wavenumber-integration (W-INT) synthetics bandpass filtered between 0.5 and 2 Hz for an NTS model. The top four traces are for a synthetic earthquake at 5 km depth, and final synthetics are either for a monopole explosion or CLVD source. The first trace was propagated without  $Q$  while all other simulations had attenuation. The models were either homogenous (e.g.,  $A_x=A_y=A_z=0$ ) or stochastic with 2 km correlation lengths. All GFM simulations were for 3D models while W-INT solutions were for a 1D homogenous slice of the NTS model. Also shown are the records for the nuclear explosion Mast at MNV. The  $L_g$  group velocity window is shown in gray.

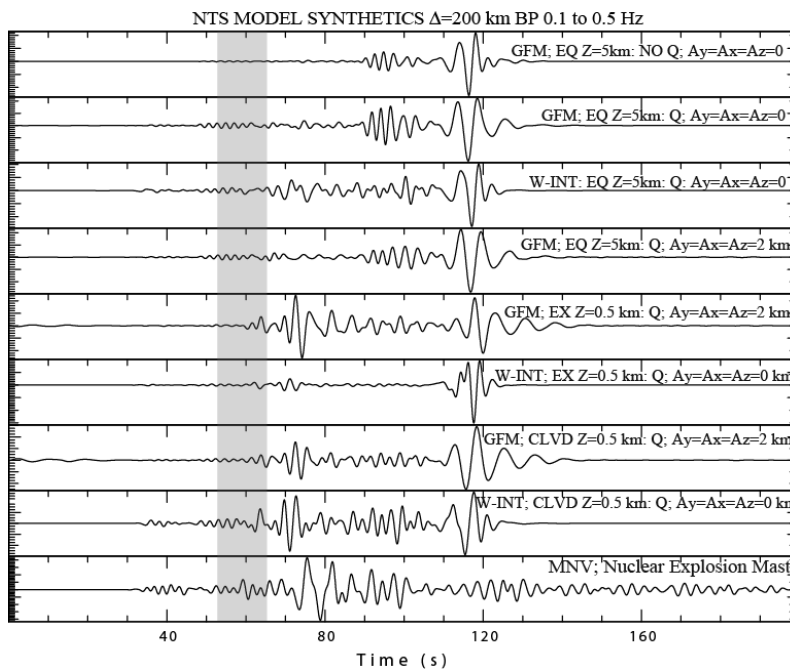


Figure 6. 3D GFM and 1D wavenumber-integration (W-INT) synthetics bandpass filtered between 0.1 and 0.5 Hz for an NTS model. See Figure 5 caption for further explanation.

### Re-Evaluation of the Haskell Source with Application to Small Explosions

The theoretical derivation of explosion source time-functions begins with Sharpe (1942) among others. Today, the most popular explosion source theory is arguably the Mueller-Murphy (1971) model, which was based on the initial source theory of Sharpe and free-field observations from the NTS to develop an analytic approximation to the pressure field acting at the elastic radius. The Mueller-Murphy model has been shown to predict the source characteristics of nuclear explosions as well as smaller chemical and mining explosions.

In the process of porting the Harkrider (1964) synthetics programs into our synthetic calculations, we reviewed the available explosion source theories for inclusion in the new software package. We included the Haskell (1961) static source theory. Primarily interested in decoupling, Haskell assumed that the source region was composed of a vaporization region surrounded by the containment media, which behaved elastically beyond the elastic radius ( $r_2$ ). Inside the elastic radius to the vapor radius ( $r_o$ ), a region of stress greater than the plastic yield stress is governed by the Coulomb-Mohr yield criteria. During the explosion, the plastic state of the material is forced by the expanding gasses out to a radius, which is assumed to be the observed cavity radius ( $r_1$ ). This formulation requires the explosive yield, the ratio of the vapor to the cavity radius, and a plastic parameter that is a simple function the Coulomb coefficient of friction and the tensile strength of the material, to obtain a unique solution. This solution, predicts the vapor, cavity and elastic radii as well as  $\psi_\infty$ . This solution, predicts the vapor, cavity and elastic radii as well as the steady-state estimate of the reduced displacement potential (e.g.,  $\psi_\infty$ ).

The equation used to determine  $\psi_\infty$ ,  $r_1$ , and  $r_2$  as functions of  $r_o$  is:

$$\left(\frac{r_o}{r_1}\right)^3 = 1 - \frac{3k(\sigma_1 + P_o)}{\mu(3-k)}\left(\frac{r_2}{r_1}\right)^3 - \frac{3(\sigma_1 + P_o)}{(3\lambda + 2\mu)} \left[ 1 + \frac{4k}{3-k}\left(\frac{r_2}{r_1}\right)^3 - \frac{3(1+k)}{3-k}\left(\frac{r_2}{r_1}\right)^m \right], \quad (2)$$

where  $\sigma_1$  is a principal stress,  $k$  is internal friction,  $m = 4k/(1+k)$ ,  $\lambda$  and  $\mu$  are Lamé's constants, and  $P_o$  is the static or overburden pressure. The corresponding initial radius is then computed as:

$$r_o^3 = \frac{3(\gamma-1)W}{4\pi P} \left(\frac{r_o}{r_1}\right)^{3\gamma}, \quad (3)$$

where  $\gamma$  is the specific heat ratio of the gas,  $W$  is the explosion yield, and  $P$  is the final cavity pressure.  $\psi_\infty$  is estimated with the equation:

$$\psi_\infty = \frac{r_2^3 k(\sigma_1 + P_o)}{\mu(3-k)}. \quad (4)$$

Haskell used his formulation for the Cowboy experiments and the contained Rainier event. Since then, seismic moment, cavity radius, and corner frequency for NTS events have been regressed by Denny and Johnson (1991) as a function of yield and elastic confinement media constants. The Haskell solution of the Rainier event, assuming the calculated or observed ratio of the vapor to cavity radii, agreed remarkably well with the regression values (Table 1). Since the relation between explosion moment and  $\psi_\infty$  had not been defined in 1961, we used the Haskell and elastic radius to calculate the moment and the corner frequency from the elastic radius and body velocity.

**Table 1. Comparison of Haskell (1961) versus Denny and Johnson (1991) results for the NTS event Rainier**

Parameter	Haskell (1961)	Denny and Johnson (1991)	%Difference
Cavity Radius (m)	18.6	17.9	3.9
Moment (N-m)	2.4E14	2.7E14	11.1
Corner Frequency (Hz)	1.9	2.1	9.5

The Haskell (1961) theory is most useful for predicting  $\psi_\infty$  and the corner-frequency and is basically a tool for surface wave and  $M_s$  calculations. Although, assuming that the pressure history on the cavity wall is a step function,

one can obtain a reduced displacement history for which  $\psi_\infty$  is the long time value for use in body wave  $m_b$  calculations.

We have modeled small chemical explosions in limestone and granite (Table 2) using the Haskell (1961) source. Haskell proposed that his method could be applied to chemical explosions and that  $r_o$  would be equal to the radius of the explosive charge. Since Denny and Johnson (1991) and Haskell (1961) agreed on the cavity radius for Rainier, we used Denny and Johnson (1991) to estimate  $r_c$  for the chemical explosions, which provided us with the  $r_o/r_c$  needed for the Haskell (1961) source.

**Table 2. Parameters used to model chemical explosions using the Haskell (1961) explosion source.**

Test Case 1	Arizona Coal Mine	Arizona Copper Mine
Medium	Limestone	Granodiorite
Chemical Explosion Yields	200 lbs – 13,807 lbs	1700 lbs – 13,600 lbs
Charge Radius (ro)	0.1 m	0.1 m
$V_p/V_s$	3.35 : 0.83 km/sec	5 km/sec
Emplacement Depths	13-35 meters	13-33 meters
Observed $M_w$ s	Yang and Bonner (2009) moment tensor inversions	Zhou et al. (2005) moment tensor inversions

We predicted  $M_w$  within 5% of the observed  $M_w$  for fully-confined shots in limestone (Figure 7) when using the Haskell (1961) source theory to estimate  $\psi_\infty$  and Denny and Johnson (1991) to estimate cavity radius ( $r_l$ ). It is interesting to note that the Denny and Johnson (1991) predicted  $M_w$ s, based on regression results from NTS, are off by 8–14% (smaller than observed). For the unconfined shots, which exhibited retard (crater spelled backwards), the predicted  $M_w$ s were 8–12% larger than observed. For the free face shots, the predicted  $M_w$ s were 10–22% larger than observed.

We predicted  $M_w$  within 2–7% of the observed  $M_w$  for fully-confined shots in granodiorite (Figure 7). The Denny and Johnson (1991) predicted  $M_w$ s varied from the observed by 8–11%. As expected, Haskell (1961) overpredicts the  $M_w$  for free face and unconfined shots, which produced blowout craters, by more than 12%.

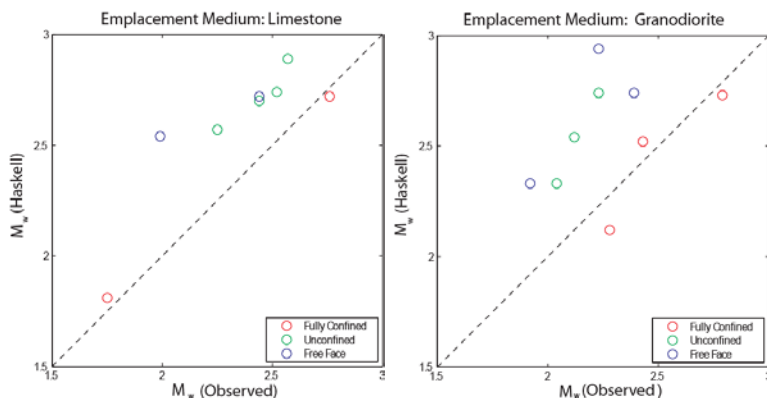


**Figure 7. Predicted  $M_w$ s using the Haskell (1961) static explosion source theory and explosion parameters in limestone (left) and granodiorite (right).**

**CONCLUSIONS AND RECOMMENDATIONS**

In the remaining months of this project, we will finalize our 3D deterministic and stochastic simulations for the NTS model. We will then convolve the monopole and CLVD Green's functions with the reduced displacement potentials from either the Mueller and Murphy (1971) or Haskell (1961) sources. We will then compare the resulting synthetics to observed seismic data from NTS explosions. We also hope to be able to add topography to these models, which Myers (2007) has shown to be an important source of explosion-generated S-waves.

### ACKNOWLEDGEMENTS

We wish to thank John Davies for assistance on the code development and Anastasia Stroujkova for help with model development.

### REFERENCES

- Benz, H. M., Unger, J. D., Leith, W. and V. Ryaboy (1991). The Norilsk DSS Profile in Northern Siberia: Interpretation of the velocity structure and comparison with Basin and Range and New England profiling results, Abstracts of the 13th Annual PL/DARPA Seismic Research Symposium: 85–100.
- Bonner, J. L., A. Stroujkova, and K. Mayeda (2008). Predicting explosion-generated  $S_n$  and  $L_g$  coda using synthetic seismograms. in *Proceedings of the 30th Monitoring Research Review: Ground-Based Nuclear Explosion Monitoring Technologies*, LA-UR-08-05261, Vol. 1, pp. 10–19.
- Denny, M.D. and L. R. Johnson (1991). The explosion seismic source function: model and scaling laws revisited, in H.J. Patton and P.G. Richards, Eds., *Explosion Source Phenomenology*, Geophysics Monograph 65, American Geophysical Union, Washington, 1–24.
- Emmerich, H. and M. Korn (1987). Incorporation of attenuation and time-domain components of seismic wave fields, *Geophys.* 52: 1252–1264.
- Harkrider, D.G. (1964). Surface waves in multilayered elastic media I. Rayleigh and Love waves from buried sources in a multilayered elastic half-space. *Bull. Seism. Soc. Am.* 54: 627–679.
- Haskell, N. (1961). A static theory of the seismic coupling of a contained underground nuclear explosion, *J. Geophys. Res.*: 3297.
- Herrmann, R. H. (2002). An overview of synthetic seismogram computation. In *Computer Programs in Seismology, Version 3.30*.
- Jih, R. S. (1998). Location calibration efforts in China, in *Proc. 20th Annual Seismic Research Symposium on Monitoring a Comprehensive Test Ban Treaty*, 21–23 September 1998: 44–55.
- Levin, V., W.-Y. Kim, and W. Menke (1995). Seismic velocities in the shallow crust of western New England and northern New York, *Bull. Seism. Soc. Am.* 85: 207–219.
- Li, S., and W. D. Mooney (1998). Crustal structure of China from deep seismic sounding profiles, *Tectonophysics* 288: 105–113.
- Myers, S.C. (2007). Numerical experiments investigating the source of explosion S-waves. *Seism. Res. Letts.* 78: 240.
- Mueller, R. A. and J. R. Murphy, (1971). Seismic characteristics of underground nuclear detonations: Part I, Seismic scaling law of underground detonations, *Bull. Seism. Soc. Am.* 61: 1675.
- Orrey, J. L., (1995). A generalized Fourier pseudospectral method for elastodynamics. Ph. D. Thesis. University of Colorado, Boulder.
- Patton, H.J. and S. R. Taylor, (1994).  $Q$  structure of the Basin and Range from surface waves, *J. Geophys. Res.* 89: 6929–6940
- Sharpe, J. A., (1942). The production of elastic waves by explosion pressures: I, Theory and Empirical field observations, *Geophys.* 7: 144.
- Tibuleac, I. M., A. Stroujkova, J. L. Bonner, K. Mayeda, and J. Britton (2006). Predicting explosion generated  $L_g$  and  $S_n$  using synthetic seismograms, in *28th Seismic Research Review: Ground-Based Nuclear Explosion Monitoring Technologies*: LA-UR-06-5471, Vol. 1, pp. 283–294.
- Xie, J. R. Gok, J. Ni and Y. Aoki (2004), Lateral variations of crustal seismic attenuation along the INDEPTH Profiles in Tibet from  $L_g$   $Q$  inversion, *J. Geophys. Res.*, 109, B10308, doi:10.1029/2004JB002988.
- Xie, J., Z. Wu, D. Schaff, Y. Liu, and J. Liang (2006). Tomographic regionalization of crustal  $L_g$   $Q$  in eastern Eurasia. *Geophys. Res. Letts*, 33, L03315, doi. 1029/2005GL024410.
- Yang, X. and J. L. Bonner (2009). Characteristics of chemical explosive sources from time-dependent moment tensors. *Bull. Seism. Soc. Am.* 99: 36–51.
- Yang, X. (2002). A numerical investigation of  $L_g$  geometrical spreading. *Bull. Seism. Soc. Am.* 92: 3067–3079.
- Zhou, R., B. W. Stump and X. Yang (2005). Moment tensor inversions of single-fired mining explosions at a copper mine in Arizona, *Eos Trans. AGU*, 86(52), Fall Meet. Suppl., Abstract S11B–0166.